Journal of Sound and Vibration (2002) **257**(3), 559–583
doi:10.1006/jsvi.5059, available online at http://www.idealibrary.com on IDEAL®

MODELLING OF TRANSVERSE VIBRATION OF SHORT BEAMS FOR CRACK DETECTION AND MEASUREMENT OF CRACK EXTENSION

S. P. Lele and S. K. Maiti

Department of Mechanical Engineering, Indian Institute of Technology Bombay, Powai, Mumbai 400076, *India. E-mail: skmaiti@me.iitb.ac.in*

(*Received* 10 *August* 2001, *and in final form* 19 *December* 2001)

The method of detection of location of crack in beams based on frequency measurements is extended here to short beams, taking into account the effects of shear deformation and rotational inertia through the Timoshenko beam theory and representing the crack by a rotational spring. Methods for solving both forward (determination of frequencies of beams knowing the crack parameters) and inverse (determination of crack location knowing the natural frequencies) problems are included. A method to estimate crack extension from a change in the first natural frequency is presented. Both numerical and experimental studies are given to demonstrate the accuracy of the methods. The accuracy of the results is quite encouraging.

1. INTRODUCTION

Machines and structural components require continuous monitoring for the detection of cracks and crack growth for ensuring an uninterrupted service. Non-destructive testing methods like ultrasonic testing, X-ray, etc., are generally useful for the purpose. These methods are costly and time consuming for long components, e.g., railway tracks, long pipelines, etc. Vibration-based methods can offer advantages in such cases. This is because measurement of vibration parameters like natural frequencies is easy. Further, this type of data can be easily collected from a single point of the component. This factor lends some advantages for components which are not fully accessible. This also helps to do away with the collection of experimental data from a number of data points on a component, which is involved in a prediction based on, for example, mode shapes.

Several approaches have been used for modelling a crack in a beam. In one method, the crack is modelled by appropriately reducing the section modulus [1]. In another approach, the crack is modelled by a local flexibility matrix. Dimarogonas and Papadopoulos [2] have given a complete 6×6 compliance matrix, including off-diagonal terms for coupling of various types (longitudinal, transverse, etc.) of vibration. In the case of pure bending vibration of beams, only the bending compliance is important. The crack can then be represented by a rotational spring [3, 4].

Some investigators have modified the Euler–Bernoulli beam equation to take into account the effect of a crack. Christides and Barr [5] have developed a cracked Euler–Bernoulli beam theory. They have considered an exponential decay in the stress field due to the crack and incorporated the effect by introducing a parameter which is to be evaluated by experiments. Chondros and Dimarogonas [6] have developed a continuous cracked beam vibration theory. They consider that the crack introduces a continuous

0022-460X/02/$35.00

change in flexibility in its neighbourhood and model it by incorporating a displacement field consistent with the singularity.

A finite element method (FEM) has also been used for study of the vibration of cracked components. A quarter point element is utilized for modelling the region around the crack, which correctly models the square-root singularity in the stress field [7]. Gounaris and Dimarogonas [8] have developed a finite element for a cracked prismatic beam for structural analysis based on the compliance matrix for the crack.

The vibration parameters of a beam change whenever its geometry changes due to a crack. Some of these parameters have been used for the detection of crack location and size, i.e., to address the inverse problem. Rizos *et al.* [4] have proposed a method based on the flexural vibration of uniform beams by representing the crack section by a rotational spring. The method needs measurement of amplitudes at any two locations along the beam. Liang *et al.* [9] have given a method similar to the above, but it requires measurement of three transverse natural frequencies of the beam. The method has been extended to stepped beams [10], cantilever beams with inclined edge cracks and internal cracks [11], geometrically segmented beams [12], etc. There is a need to see if this approach can be used for short beams, where the effects of shear deformation and rotational inertia are not negligible. An investigation has been reported by Tsai and Wang [13] accommodating these effects. However, the basis for their crack detection is the mode shape rather than the natural frequency. There is a very limited data concerning experimental observations too. These have provided some motivation for the present study.

The vibration-based methods, irrespective of whether the basis is the mode shape or frequency, have so far been intended for exploitation for detection of cracks. The issue of detection of crack extension has not yet been looked into. If this can also be brought within its scope, its practical utility will enhance considerably. Collection of fatigue crack growth data via laboratory testing requires the measurement of crack extension frequently. This is done using a three-point bend (TPB) specimen or a compact tension (CT) specimen. Currently, electric potential technique and compliance method are employed for the measurement of crack extension. Out of the two configurations, the TPB specimen, which has the geometry of a short beam, is more suited for the application of the vibration method. The possibility of using the vibration-based method is open to investigations. This has also provided some motivation for the present study.

The objective of this paper is to extend the frequency-based methods of crack detection to short beams by taking into account the effects of rotational inertia and shear deformation. Methods for solving both the forward and inverse problems are presented. The forward problem involves determination of natural frequencies from the knowledge of beam geometry and crack parameters. The inverse problem concerns prediction of crack location for a given beam geometry from the knowledge of its natural frequencies. A method to estimate the crack extension from changes in natural frequency of the first mode of vibration is also given. Case studies, both numerical and experimental, are presented to demonstrate the effectiveness of the methods.

2. FORMULATION

A crack located at distance L_1 from the fixed end of a cantilever (Figure 1) is represented by a rotational spring of stiffness K_t, whose magnitude is given by [14]

$$K_t = \frac{EBW^4}{72\pi \int_0^a a(f(a/W))^2 \, \mathrm{d}a}, \tag{1}$$

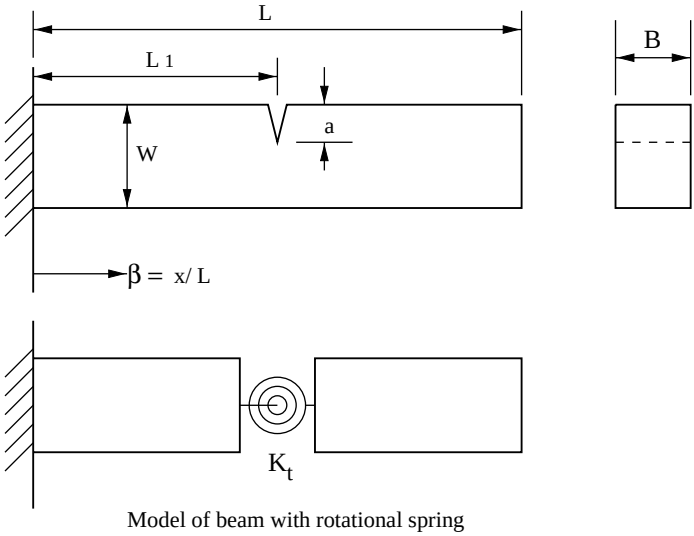

Figure 1. Short beam with a crack.

where $f(a/W)$ is given by [12]

$$\left[f\left(\frac{a}{W}\right)\right]^2 = a\left(1{\cdot}2769 - 3{\cdot}105\,\frac{a}{W} + 14{\cdot}878\,\frac{a^2}{W^2} - 25{\cdot}8\,\frac{a^3}{W^3} + 45{\cdot}32\,\frac{a^4}{W^4}\right.$$
$$- 51{\cdot}33\,\frac{a^5}{W^5} + 64{\cdot}39\,\frac{a^6}{W^6} - 62{\cdot}96\,\frac{a^7}{W^7} + 200{\cdot}9\,\frac{a^8}{W^8} - 243{\cdot}2\,\frac{a^9}{W^9}$$
$$\left. + 83{\cdot}16\,\frac{a^{10}}{W^{10}} + 225{\cdot}6\,\frac{a^{12}}{W^{12}}\right). \tag{2}$$

The governing equations of flexural vibration are given by Timoshenko [15] as follows:

$$EI\,\frac{\partial^2\psi}{\partial x^2} + k'\left(\frac{\partial y}{\partial x} - \psi\right)AG - \rho I\,\frac{\partial^2\psi}{\partial t^2} = 0, \tag{3}$$

$$\rho\,\frac{\partial^2 y}{\partial t^2} - k'\left(\frac{\partial^2 y}{\partial x^2} - \frac{\partial\psi}{\partial x}\right)G = 0, \tag{4}$$

where y is the transverse deflection, ψ the angle of rotation due to bending moment, E the modulus of elasticity, G the modulus of rigidity, A the area of cross-section, I the area moment of inertia, ρ the density and k' the numerical shape factor for the cross-section.

Following Huang [16], the solutions for these equations can be written in the following form:

$$Y = A_1\cosh bp\beta + A_2\sinh bp\beta + A_3\cos bq\beta + A_4\sin bq\beta, \tag{5}$$

$$\Psi = A'_1\sinh bp\beta + A'_2\cosh bp\beta + A'_3\sin bq\beta + A'_4\cos bq\beta, \tag{6}$$

where Y is the amplitude function of y, and Ψ the amplitude function of ψ,

$$\beta = \frac{x}{L}, \qquad b^2 = \frac{\rho A L^4 \omega^2}{EI}, \qquad r^2 = \frac{1}{AL^2}, \qquad s^2 = \frac{EI}{k' AGL^2} \tag{7–9}$$

and

$$\left.\begin{matrix} P \\ q \end{matrix}\right\} = \frac{1}{\sqrt{2}} [\, \mp (r^2 + s^2) + [(r^2 - s^2)^2 + 4/b^2]^{1/2}]^{1/2} \tag{10}$$

provided

$$[(r^2 - s^2)^2 + 4/b^2]^{1/2} > (r^2 + s^2). \tag{11}$$

If the above condition is not satisfied then

$$p' = \mathrm{j} \frac{1}{\sqrt{2}} [(r^2 + s^2) - [(r^2 - s^2)^{\,2} + 4/b^2]^{1/2}]^{1/2} \tag{12}$$

and the solutions are given by

$$Y = A_1 \cos bp'\beta + \mathrm{j}A_2 \sin bp'\beta + A_3 \cos bq\beta + A_4 \sin bq\beta, \tag{13}$$

$$\Psi = \mathrm{j}A'_1 \sin bp'\beta + A'_2 \cos bp'\beta + A'_3 \sin bq\beta + A'_4 \cos bq\beta. \tag{14}$$

A_i and A'_i are arbitrary constants to be determined from the boundary conditions. Only four of these constants are independent and the relations between them are given by

$$A'_1 = \frac{b}{L} \frac{p^2 + s^2}{p} A_1, \tag{15}$$

$$A'_2 = \frac{b}{L} \frac{p^2 + s^2}{p} A_2, \tag{16}$$

$$A'_3 = -\frac{b}{L} \frac{q^2 - s^2}{q} A_3, \tag{17}$$

$$A'_4 = \frac{b}{L} \frac{q^2 - s^2}{q} A_4. \tag{18}$$

For a cracked beam (Figure 1), the two segments lying on either side of the crack can be analyzed separately. The solutions for the two segments can be written as follows:

$$Y_1 = C_1 \cosh bp\beta + C_2 \sinh bp\beta + C_3 \cos bq\beta + C_4 \sin bq\beta, \tag{19}$$

$$\Psi_1 = C'_1 \sinh bp\beta + C'_2 \cosh bp\beta + C'_3 \sin bq\beta + C'_4 \cos bq\beta, \tag{20}$$

$$Y_2 = C_5 \cosh bp\beta + C_6 \sinh bp\beta + C_7 \cos bq\beta + C_8 \sin bq\beta, \tag{21}$$

$$\Psi_2 = C'_5 \sinh bp\beta + C'_6 \cosh bp\beta + C'_7 \sin bq\beta + C'_8 \cos bq\beta. \tag{22}$$

The condition given by (equation (11)) is always satisfied for the cases considered in the present study. The relations between constants C_i and C'_i, in the above equations for Y and Ψ are given by

$$C'_i = \frac{b}{L}\frac{p^2 + s^2}{p} C_i \quad \text{for } i = 1, 2, 5, 6, \tag{23}$$

$$C'_i = -\frac{b}{L}\frac{q^2 - s^2}{q} C_i \quad \text{for } i = 3, 7, \tag{24}$$

$$C'_i = \frac{b}{L}\frac{q^2 - s^2}{q} C_i \quad \text{for } i = 4, 8. \tag{25}$$

The boundary conditions for a cantilever beam fixed at the left end are as follows:

$$Y_1|_{\beta=0} = 0 \quad \text{and} \quad \Psi_1|_{\beta=0} = 0, \tag{26}$$

$$\left.\frac{\mathrm{d}\Psi_2}{\mathrm{d}\beta}\right|_{\beta=1} = 0 \quad \text{and} \quad \left.\frac{1}{L}\frac{\mathrm{d}Y_2}{\mathrm{d}\beta}\right|_{\beta=1} - \Psi_2|_{\beta=1} = 0. \tag{27}$$

The conditions for continuity of displacement, moment and shear force at the crack location and the jump in the slope can be written, respectively, in the following form:

$$Y_1 = Y_2, \tag{28}$$

$$\frac{\mathrm{d}\Psi_1}{\mathrm{d}\beta} = \frac{d\Psi_2}{d\beta}, \tag{29}$$

$$\frac{1}{L}\frac{\mathrm{d}Y_1}{\mathrm{d}\beta} - \Psi_1 = \frac{1}{L}\frac{\mathrm{d}Y_2}{\mathrm{d}\beta} - \Psi_2, \tag{30}$$

$$\frac{\mathrm{d}Y_1}{\mathrm{d}\beta} + \frac{L}{K}\frac{\mathrm{d}\Psi_1}{\mathrm{d}\beta} = \frac{\mathrm{d}Y_2}{\mathrm{d}\beta}, \tag{31}$$

where $K = K_t L/EI$ is the non-dimensional stiffness of the rotational spring representing the crack.

Since there is continuity of the shear force at the crack site, the angle of shear ϕ on both the sides will be the same. Therefore, the change in slope $\mathrm{d}Y/\mathrm{d}x$ will be equal to the change in the slope Ψ due to bending only. So the jump condition can be written in terms of Ψ:

$$\Psi_1 + \frac{1}{K}\frac{\mathrm{d}\Psi_1}{\mathrm{d}\beta} = \Psi_2. \tag{32}$$

From the above four boundary conditions and four compatibility equations (equations (28)–(31)), the following characteristic equation is obtained:

$$
\begin{vmatrix}
1 & 0 & 1 & 0 \\
0 & \dfrac{p^2+s^2}{p} & 0 & \dfrac{q^2-s^2}{q} \\
0 & 0 & 0 & 0 \\
0 & 0 & 0 & 0 \\
\cosh bp\beta^* & \sinh bp\beta^* & \cos bq\beta^* & \sin bq\beta^* \\
(p^2+s^2)\cosh bp\beta^* & (p^2+s^2)\sinh bp\beta^* & -(q^2-s^2)\cos bq\beta^* & -(q^2-s^2)\sin bq\beta^* \\
\dfrac{-s^2}{p}\sinh bp\beta^* & \dfrac{-s^2}{p}\cosh bp\beta^* & \dfrac{-s^2}{q}\sin bq\beta^* & \dfrac{s^2}{q}\cos bq\beta^* \\
[Kp\sinh bp\beta^* & [Kp\cosh bp\beta^* & [-Kq\sin bq\beta^* & [Kq\cos bq\beta^* \\
+b(p^2+s^2)\cosh bp\beta^*] & +b(p^2+s^2)\sinh bp\beta^*] & -b(q^2-s^2)\cos bq\beta^*] & -b(q^2-s^2)\sin bq\beta^*] \\
0 & 0 & 0 & 0 \\
0 & 0 & 0 & 0 \\
(p^2+s^2)\cosh bp & (p^2+s^2)\sinh bp & -(q^2-s^2)\cos bq & -(q^2-s^2)\sin bq \\
\dfrac{-s^2}{p}\sinh bp & \dfrac{-s^2}{p}\cosh bp & \dfrac{-s^2}{q}\sin bp & \dfrac{s^2}{q}\cos bp \\
-\cosh bp\beta^* & -\sinh bp\beta^* & -\cos bq\beta^* & -\sin bq\beta^* \\
-(p^2+s^2)\cosh bp\beta^* & -(p^2+s^2)\sinh bp\beta^* & (q^2-s^2)\cos bq\beta^* & (q^2-s^2)\sin bq\beta^* \\
\dfrac{s^2}{p}\sinh bp\beta^* & \dfrac{s^2}{p}\cosh bp\beta^* & \dfrac{s^2}{q}\sin bq\beta^* & \dfrac{-s^2}{q}\cos bq\beta^* \\
-Kp\sinh bp\beta^* & -Kp\cosh bp\beta^* & Kq\sin bq\beta^* & -Kq\cos bq\beta^*
\end{vmatrix} = 0. \quad (33)
$$

The alternative condition for jump in slope (equation (32)) can also be used instead of equation (31) to get a characteristic equation. Both these equations are used later in the case studies and found to give exactly the same results.

2.1. FORWARD PROBLEM

For the determination of the natural frequencies for a given crack location and size, the rotational spring stiffness is given as input. The characteristic equation (33) is solved to

get the frequency parameter b. In turn, the natural frequency ω is determined using equation (7).

2.2. INVERSE PROBLEM

The characteristic equation (33) for the Timoshenko beam with a crack can be rewritten in the form

$$K = -\frac{|\Delta_1|}{|\Delta_2|}, \tag{34}$$

where $|\Delta_1|$ and $|\Delta_2|$ are given by

$$|\Delta_1| = \begin{vmatrix} 1 & 0 & 1 & 0 \\ 0 & \dfrac{p^2+s^2}{p} & 0 & \dfrac{q^2-s^2}{q} \\ 0 & 0 & 0 & 0 \\ 0 & 0 & 0 & 0 \\ \cosh bp\beta^* & \sinh bp\beta^* & \cos bq\beta^* & \sin bq\beta^* \\ (p^2+s^2)\cosh bp\beta^* & (p^2+s^2)\sinh bp\beta^* & -(q^2-s^2)\cos bq\beta^* & -(q^2-s^2)\sin bq\beta^* \\ \dfrac{-s^2}{p}\sinh bp\beta^* & \dfrac{-s^2}{p}\cosh bp\beta^* & \dfrac{-s^2}{q}\sin bq\beta^* & \dfrac{s^2}{q}\cos bq\beta^* \\ b(p^2+s^2)\cosh bp\beta^* & b(p^2+s^2)\sinh bp\beta^* & -b(q^2-s^2)\cos bq\beta^* & -b(q^2-s^2)\sin bq\beta^* \end{vmatrix}$$

$$\begin{vmatrix} 0 & 0 & 0 & 0 \\ 0 & 0 & 0 & 0 \\ (p^2+s^2)\cosh bp & (p^2+s^2)\sinh bp & -(q^2-s^2)\cos bq & -(q^2-s^2)\sin bq \\ \dfrac{-s^2}{p}\sinh bp & \dfrac{-s^2}{p}\cosh bp & \dfrac{-s^2}{q}\sin bp & \dfrac{s^2}{q}\cos bp \\ -\cosh bp\beta^* & -\sinh bp\beta^* & -\cos bq\beta^* & -\sin bq\beta^* \\ -(p^2+s^2)\cosh bp\beta^* & -(p^2+s^2)\sinh bp\beta^* & (q^2-s^2)\cos bq\beta^* & (q^2-s^2)\sin bq\beta^* \\ \dfrac{s^2}{p}\sinh bp\beta^* & \dfrac{s^2}{p}\cosh bp\beta^* & \dfrac{s^2}{q}\sin bq\beta^* & \dfrac{-s^2}{q}\cos bq\beta^* \\ 0 & 0 & 0 & 0 \end{vmatrix} \tag{35}$$

and

$$|\Delta_2| = \begin{vmatrix} 1 & 0 & 1 & 0 \\ 0 & \dfrac{p^2+s^2}{p} & 0 & \dfrac{q^2-s^2}{q} \\ 0 & 0 & 0 & 0 \\ 0 & 0 & 0 & 0 \\ \cosh bp\beta^* & \sinh bp\beta^* & \cos bq\beta^* & \sin bq\beta^* \\ (p^2+s^2)\cosh bp\beta^* & (p^2+s^2)\sinh bp\beta^* & -(q^2-s^2)\cos bq\beta^* & -(q^2-s^2)\sin bq\beta^* \\ \dfrac{-s^2}{p}\sinh bp\beta^* & \dfrac{-s^2}{p}\cosh bp\beta^* & \dfrac{-s^2}{q}\sin bq\beta^* & \dfrac{s^2}{q}\cos bq\beta^* \\ p\sinh bp\beta^* & p\cosh bp\beta^* & -q\sin bq\beta^* & q\cos bq\beta^* \end{vmatrix}$$

$$\begin{vmatrix} 0 & 0 & 0 & 0 \\ 0 & 0 & 0 & 0 \\ (p^2+s^2)\cosh bp & (p^2+s^2)\sinh bp & -(q^2-s^2)\cos bq & -(q^2-s^2)\sin bq \\ \dfrac{-s^2}{p}\sinh bp & \dfrac{-s^2}{p}\cosh bp & \dfrac{-s^2}{q}\sin bp & \dfrac{s^2}{q}\cos bp \\ -\cosh bp\beta^* & -\sinh bp\beta^* & -\cos bq\beta^* & -\sin bq\beta^* \\ -(p^2+s^2)\cosh bp\beta^* & -(p^2+s^2)\sinh bp\beta^* & (q^2-s^2)\cos bq\beta^* & (q^2-s^2)\sin bq\beta^* \\ \dfrac{s^2}{p}\sinh bp\beta^* & \dfrac{s^2}{p}\cosh bp\beta^* & \dfrac{s^2}{q}\sin bq\beta^* & \dfrac{-s^2}{q}\cos bq\beta^* \\ -p\sinh bp\beta^* & -p\cosh bp\beta^* & q\sin bq\beta^* & -q\cos bq\beta^* \end{vmatrix}. \quad (36)$$

The method of Nandwana and Maiti [11] is utilized to obtain the solution. For each mode, the variation of the non-dimensional stiffness K with crack location β is obtained through equation (34). Since the rotational spring stiffness representing the crack is independent of the vibration mode, the point of intersection of three (minimum) curves gives the location of the crack. For each mode, the zero setting [10] is a must.

2.3. CRACK EXTENSION MEASUREMENT

In this case, the objective is to estimate $\Delta a = a_2 - a_1$, from the knowledge of ω_2 and ω_1, which correspond to crack lengths a_2 and a_1 respectively. The starting crack length a_1 is specified.

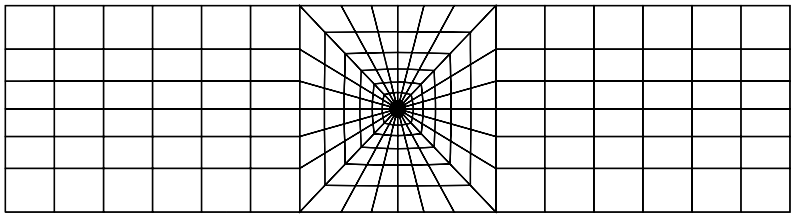

Figure 2. Finite element descritization.

For the starting crack length a_1, the rotational spring stiffness can be calculated using equation (1). The natural frequency $\bar{\omega}_1$ can then be found out by solving the characteristic equation (equation (33)). This frequency $\bar{\omega}_1$ generally differs from ω_1. In order to get an accurate estimate of the crack extension, or an estimate of a_2 corresponding to ω_2, these two values must be the same. This is ensured as follows.

From the dimensionless parameters b and s (equations (7) and (9)), it is clear that s is independent of material properties as E and G are related and b depends on ρ and E. If b is to remain the same for two different values of frequency, ω and $\bar{\omega}$, there is a need for adjusting either E or ρ. Choosing to adjust E, as has been done for the prediction of location of crack [10], the corrected modulus $\bar{E}$ corresponding to $\bar{\omega}$ is given by

$$\frac{\rho A L^4 \omega^2}{EI} = \frac{\rho A L^4 (\bar{\omega})^2}{\bar{E} I} \tag{37}$$

or

$$\frac{E}{\bar{E}} = \left(\frac{\omega}{\bar{\omega}}\right)^2. \tag{38}$$

In order to find out the crack length a_2 corresponding to the frequency ω_2, the conversion of ω_2 into frequency parameter b_2 must be done through equation (7) using $\bar{E}$ given by equation (38), instead of E. There is an improvement in the accuracy with this E correction. This is demonstrated through case studies.

3. NUMERICAL STUDIES

3.1. FORWARD PROBLEM

The method has been tested considering various geometric combinations and two sets of material properties. L/W ratios in the range 2–9 have been studied. The natural frequencies obtained from the present model have been compared with frequencies computed by a finite element programme [17]. The results obtained using the Euler–Bernoulli beam model are also presented to demonstrate the effect of rotational inertia and shear deformation.

The characteristic equation (33) is solved employing the Newton–Raphson technique to get the frequency parameter b, hence the natural frequency. The value of geometric shape factor k' is taken as 0·833 [15]. For the finite-element analysis, the beam is discretized mostly by eight-noded iso-parametric elements [18] (Figure 2). The crack tip is always surrounded by 24 quarter point singularity elements. The natural frequencies for the

TABLE 1

Comparison of natural frequencies by the Timoshenko beam model with FEM predictions for various L/W ratios[†]

		Natural frequencies (Hz)								
		Timoshenko beam model			FEM			% Error		
L/W	a/W	ω_1	ω_2	ω_3	ω_1	ω_2	ω_3	in ω_1	in ω_2	in ω_3
2	0·20	6836·5	24391·1	54994·0	6878·0	23296·0	55167·0	0·60	4·70	0·31
	0·35	6296·9	21104·9	53539·8	6282·4	18690·3	52812·1	0·23	12·92	1·38
	0·50	5403·9	18174·5	52348·0	5272·9	14916·3	48243·0	2·48	21·84	8·51
3	0·20	3330·6	14399·9	33827·8	3344·2	14233·3	34225·6	0·41	1·17	1·16
	0·35	3132·0	12643·6	33372·4	3135·3	11966·7	33455·7	0·11	5·66	0·25
	0·50	2782·5	10852·7	32938·0	2762·4	9653·3	32105·0	0·73	12·42	2·59
4	0·20	1948·2	9392·9	22960·1	1954·2	9364·6	23181·2	0·31	0·30	0·95
	0·35	1855·5	8387·7	22799·8	1858·4	8133·1	22909·1	0·16	3·13	0·48
	0·50	1685·1	7163·8	22629·5	1681·2	6701·5	22386·3	0·23	6·90	1·09
5	0·20	1272·4	6558·7	16566·5	1275·5	6550·8	16691·5	0·25	0·12	0·75
	0·35	1222·2	5879·6	16502·3	1224·1	5804·6	16578·4	0·16	1·29	0·46
	0·50	1127·0	5071·2	16428·3	1126·4	4873·4	16343·8	0·06	4·06	0·52
6	0·20	894·2	4814·7	12471·3	896·3	4810·6	12545·0	0·24	0·09	0·59
	0·35	864·1	4355·0	12443·6	865·4	4321·8	12492·3	0·15	0·77	0·39
	0·50	805·8	3776·3	12408·4	806·0	3681·9	12376·0	0·02	2·57	0·26
7	0·20	662·0	3672·7	9696·7	663·2	3669·6	9740·2	0·18	0·09	0·45
	0·35	642·6	3348·7	9682·7	643·5	3331·4	9713·4	0·14	0·52	0·32
	0·50	604·4	2921·2	9664·5	604·7	2871·5	9651·4	0·05	1·73	0·14
8	0·20	509·5	2887·8	7734·2	510·3	2885·1	7760·6	0·16	0·10	0·34
	0·35	496·3	2651·6	7726·7	497·0	2641·4	7746·2	0·13	0·39	0·25
	0·50	469·9	2327·3	7716·7	470·3	2299·0	7711·3	0·07	1·23	0·07
9	0·20	404·1	2326·9	6299·6	404·7	2324·4	6316·0	0·15	0·11	0·26
	0·35	394·7	2149·9	6295·3	395·2	2143·2	6307·9	0·12	0·31	0·20
	0·50	375·8	1898·3	6289·4	376·1	1881·0	6287·5	0·08	0·92	0·03

[†] $W = 25$ mm, $B = 12{\cdot}5$ mm, $E = 210$ GPa, $\rho = 7860$ kg/m^3, $v = 0{\cdot}3$, $\beta^* = 0{\cdot}5$.

Euler–Bernoulli model have been obtained by solving the appropriate characteristic equation.

The following material properties are used in the case studies unless otherwise specified: modulus of elasticity $E = 210$ GPa, density $\rho = 7860$ kg/m^3 and the Poisson ratio $v = 0{\cdot}3$. The geometric data considered are width $(W) = 25$ mm and thickness $(B) = 12{\cdot}5$ mm. The crack is assumed to be located at the centre of the beam. Table 1 gives a comparison of the first three natural frequencies by the present Timoshenko beam model with the results of the FEM for various L/W ratios. Table 2 presents a comparison of the similar predictions based on the Euler–Bernoulli beam model with FEM results for the same cases.

The results of the Timoshenko beam model are in good agreement with the FEM results in the entire range of L/W ratio. For shorter beams (lower L/W ratios), the difference between the results by the Euler–Bernoulli model and the FEM, as expected, increases. This shows the effect of rotational inertia and shear deformation. The present model predicts the first natural frequency with the highest accuracy when the FEM results are taken as the basis. The error is more in the next two modes. Further, the error decreases as the L/W ratio increases. Figure 3 shows the variation of errors in natural frequencies for the first three

TABLE 2

Comparison of natural frequencies by the Euler–Bernoulli model with FEM predictions for various L/W ratios[†]

		Natural frequencies (Hz)						% Error		
		Euler–Bernoulli			FEM					
L/W	a/W	ω_1	ω_2	ω_3	ω_1	ω_2	ω_3	in ω_1	in ω_2	in ω_3
2	0·20	7940·0	44414·0	146502·0	6878·0	23296·0	55167·0	15·44	90·65	165·56
	0·35	7249·9	36350·1	146485·0	6282·4	18690·3	52812·1	15·40	94·49	177·37
	0·50	6097·1	30676·0	146326·0	5272·9	14916·3	48243·0	15·63	105·65	203·31
3	0·20	3597·7	20669·2	65114·0	3344·2	14233·3	34225·6	7·58	45·22	90·25
	0·35	3365·4	17437·7	65107·3	3135·3	11966·7	33455·7	7·34	45·72	94·61
	0·50	2976·3	14817·0	64794·0	2762·4	9653·3	32105·0	7·74	53·49	101·82
4	0·20	2039·1	11960·3	36627·3	1954·2	9364·6	23181·2	4·35	27·72	58·00
	0·35	1936·9	10307·7	36623·9	1858·4	8133·1	22909·1	4·22	26·74	59·87
	0·50	1752·2	8654·0	36589·8	1681·2	6701·5	22386·3	4·22	29·14	63·45
5	0·20	1311·1	7762·9	23441·7	1275·5	6550·8	16691·5	2·79	18·50	40·44
	0·35	1257·6	6831·4	23439·8	1224·1	5804·6	16578·4	2·74	17·69	41·39
	0·50	1157·6	5792·3	23437·6	1126·4	4873·4	16343·8	2·77	18·86	43·40
6	0·20	913·3	5453·2	16279·1	896·3	4810·6	12545·0	1·90	13·36	29·77
	0·35	881·8	4868·6	16277·9	865·4	4321·8	12492·3	1·90	12·65	30·30
	0·50	821·3	4170·9	16277·0	806·0	3681·9	12376·0	1·90	13·28	31·52
7	0·20	672·5	4040·5	11690·2	663·2	3669·6	9740·2	1·40	10·11	20·02
	0·35	652·4	3649·4	11959·4	643·5	3331·4	9713·4	1·39	9·54	23·12
	0·50	613·0	3151·4	11958·6	604·7	2871·5	9651·4	1·37	9·75	23·91
8	0·20	515·7	3113·6	9157·1	510·3	2885·1	7760·6	1·05	7·92	17·99
	0·35	502·2	2839·0	9156·5	497·0	2641·4	7746·2	1·05	7·48	18·21
	0·50	475·1	2472·3	9157·3	470·3	2299·0	7711·3	1·04	7·54	18·75
9	0·20	408·0	2472·8	7235·3	404·7	2324·4	6316·0	0·82	6·38	14·55
	0·35	398·4	2272·5	7234·8	395·2	2143·2	6307·9	0·81	6·03	14·69
	0·50	379·1	1993·8	7234·3	376·1	1881·0	6287·5	0·81	6·00	15·06

[†] $W = 25$ mm, $B = 12{\cdot}5$ mm, $E = 210$ GPa, $\rho = 7860$ kg/m^3, $v = 0{\cdot}3$, $\beta^* = 0{\cdot}5$.

modes with L/W ratios for $a/W = 0{\cdot}5$. The results based on both the Timoshenko beam model and the Euler–Bernoulli beam model are shown.

A comparison of analytical and FEM natural frequencies for various crack locations along the beam is given in Table 3 for two L/W ratios (4 and 6). The accuracy of the prediction is the highest in the first mode for all the crack locations.

A comparison of the frequencies for different a/W ratios is presented in Table 4. These results correspond to $L = 100$ mm, $W = 25$ mm, $B = 12{\cdot}5$ mm and the crack location $\beta^* = 0{\cdot}5$. The error in the prediction is found to increase with an increase in a/W ratios. This may be partly because of an increase in error in $f(a/W)$ with an increase in a/W. The accuracy in the first natural frequency is higher around $a/W = 0{\cdot}5$.

3.2. INVERSE PROBLEM

The method for crack detection is tested for several combinations of crack sizes and crack locations. The natural frequencies calculated by the FEM are used as input in this case. The zero setting procedure given by Nandwana and Maiti [10] is applied. The variation of stiffness K with crack location β is plotted for the three modes. The intersection of the three

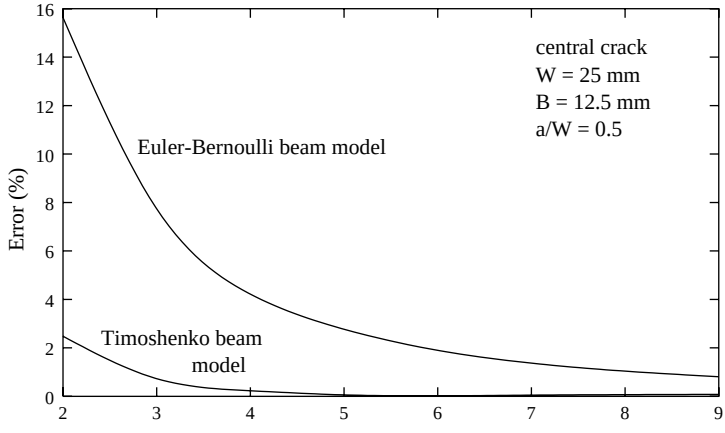

(a) Mode 1

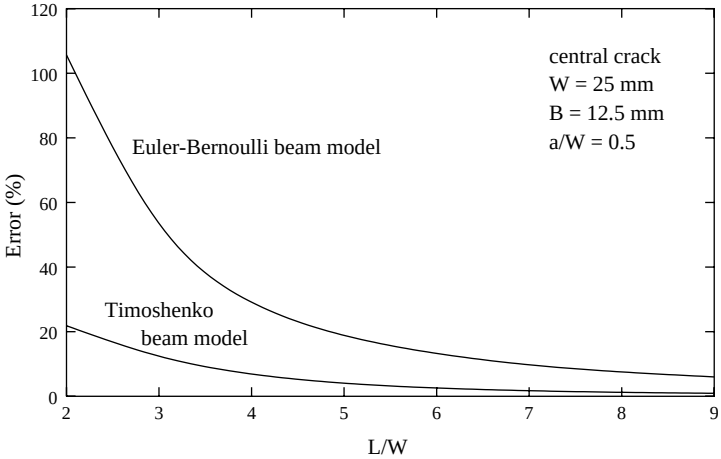

(b) Mode 2

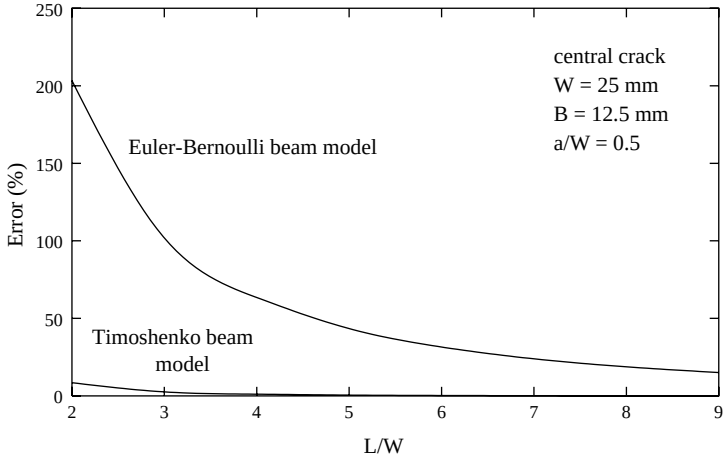

(c) Mode 3

Figure 3. Variation of error in natural frequencies with L/W ratio.

TABLE 3

Comparison of analytical and FEM natural frequencies for various crack locations

	Natural frequencies (Hz)								
	Analytical			FEM			% Error		
β^*	ω_1	ω_2	ω_3	ω_1	ω_2	ω_3	in ω_1	in ω_2	in ω_3
	$L = 100$ mm, $W = 25$ mm, $B = 12{\cdot}5$ mm, $a/W = 0{\cdot}5$								
0·2	1207·00	10073·4	21246·1	1200·98	9839·34	21433·8	0·50	2·38	0·88
0·3	1356·93	9279·88	20463·1	1349·82	8600·40	21361·7	0·53	7·90	4·21
0·4	1520·15	7997·65	22315·1	1513·96	7411·49	22268·4	0·41	7·91	0·21
0·5	1685·12	7163·82	22629·0	1681·24	6701·47	22386·3	0·23	6·90	1·08
0·6	1829·70	6960·30	19858·8	1829·36	6551·44	20065·8	0·02	6·24	1·03
0·7	1929·30	7470·71	17452·0	1932·43	7069·81	17749·9	0·16	5·67	1·68
0·8	1977·18	8732·73	16596·4	1982·38	8410·91	16529·9	0·26	3·83	0·40
0·9	1138·33	9923·01	22550·1	1137·64	9534·87	22017·6	0·06	4·07	2·42
	$L = 150$ mm, $W = 25$ mm, $B = 12{\cdot}5$ mm, $a/W = 0{\cdot}5$								
0·2	613·183	5085·45	11561·5	611·587	5033·12	11842·4	0·26	1·04	2·37
0·3	677·503	4765·15	10859·2	676·173	4671·33	11464·7	0·20	2·01	5·28
0·4	743·602	4157·69	11839·6	742·866	4048·12	11983·9	0·10	2·71	1·20
0·5	805·825	3776·34	12408·4	805·956	3681·89	12376·0	0·02	2·57	0·26
0·6	856·240	3720·78	11026·8	857·297	3638·62	11293·6	0·12	2·26	2·36
0·7	888·658	4014·11	9736·89	890·360	3946·15	10195·3	0·19	1·72	4·50

TABLE 4

Comparison of analytical and FEM natural frequencies for different a/W ratios[†]

	Natural frequencies (Hz)								
	Analytical			FEM			% Error		
a/W	ω_1	ω_2	ω_3	ω_1	ω_2	ω_3	in ω_1	in ω_2	in ω_3
0·10	1980·23	9879·87	23036·1	1987·02	9908·31	23263·1	0·34	0·29	0·98
0·20	1948·16	9392·89	22960·1	1954·17	9364·59	23181·2	0·31	0·30	0·95
0·30	1893·36	8717·61	22856·8	1897·59	8583·12	23023·2	0·22	1·57	0·72
0·35	1855·45	8387·71	22799·8	1858·43	8133·15	22909·1	0·16	3·13	0·48
0·40	1809·08	7945·27	22741·8	1810·41	7661·12	22767·4	0·07	3·71	0·11
0·50	1685·12	7163·82	22629·0	1681·24	6701·47	22386·3	0·23	6·90	1·08
0·60	1504·40	6433·65	22528·6	1493·75	5794·40	21836·7	0·71	11·03	3·17
0·70	1238·13	5794·82	22443·4	1229·48	5007·98	21044·6	0·70	15·71	6·65

[†]$L = 100$ mm, $W = 25$ mm, $B = 12{\cdot}5$ mm, $\beta^* = 0{\cdot}5$.

curves indicates the possible crack location. When the three curves do not meet exactly, the centroid of the three pairs of intersections is taken as the crack location [10]. The predicted crack locations are compared with the corresponding actual values (β^*). Since the interest lies in the detection of a crack anywhere in the whole span of the beam, it is logical to express the percentage error taking the beam length as the basis. The percentage error is therefore given by the difference between the predicted and actual crack locations expressed as a percentage of the beam length. This helps to eliminate the multiplicity of percentage

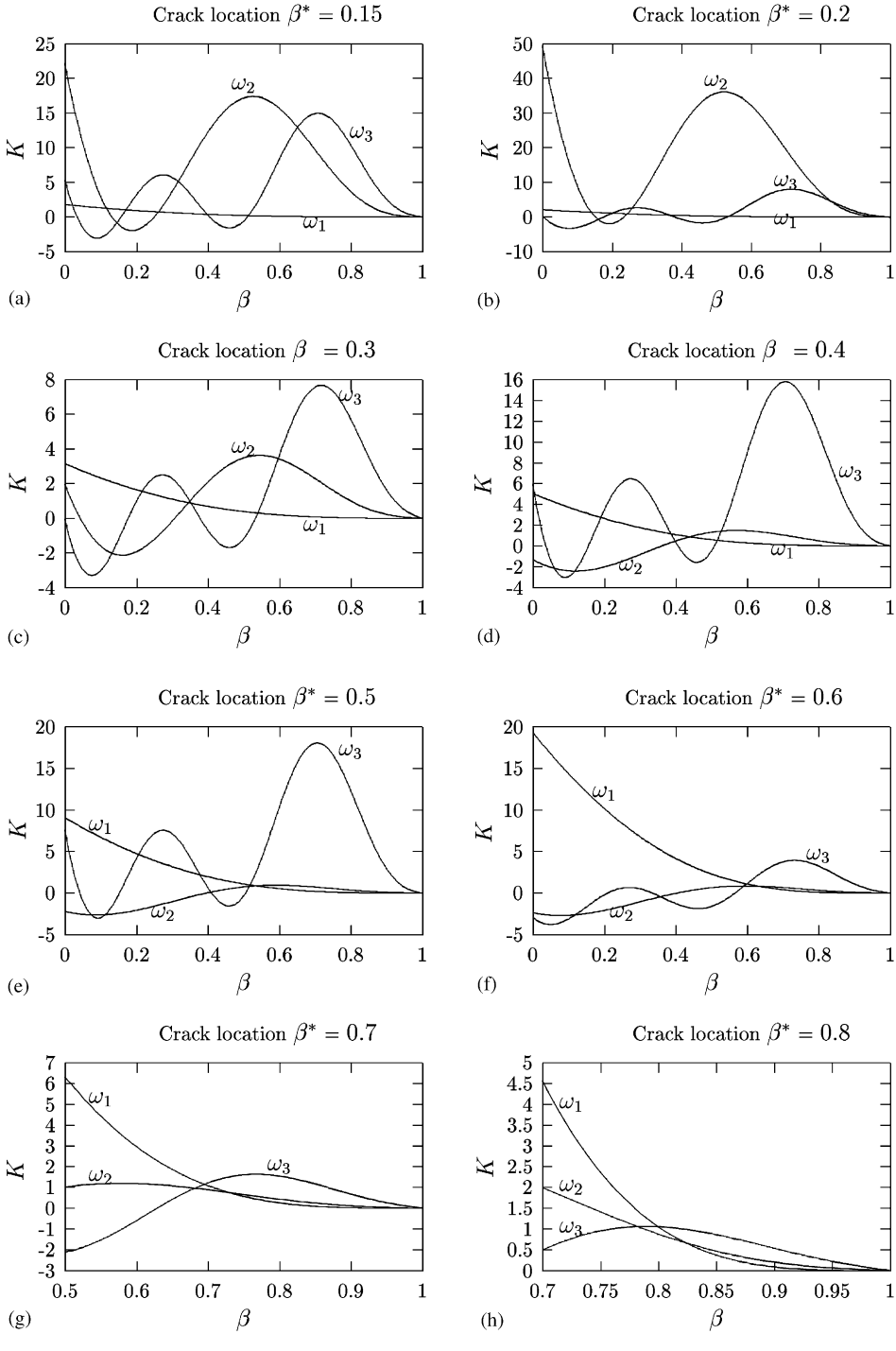

Figure 4. Plots of K vs. β for $L/W = 4$ and $a/W = 0{\cdot}5$.

errors corresponding to the same absolute difference between the predicted and actual crack locations when the latter is taken as the basis. It is found that the error in prediction of location is $< \pm 5\%$.

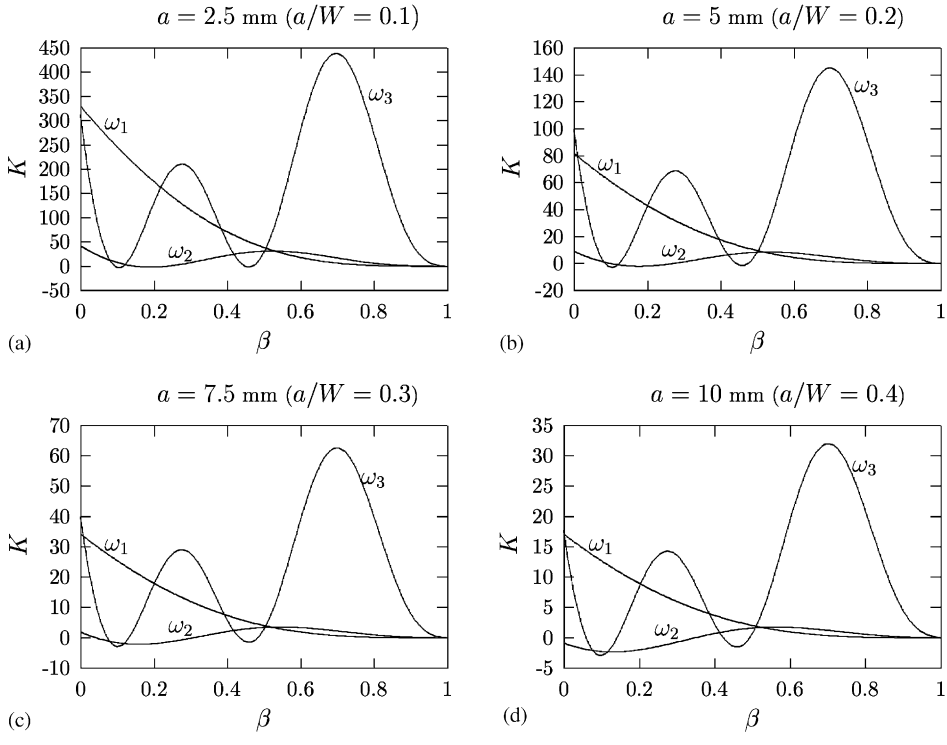

Figure 5. Plots of K vs. β for different crack sizes for $L/W = 4$ and $\beta^* = 0{\cdot}5$.

Figure 4 shows the graphs of K versus β for different crack locations corresponding to $a/W = 0{\cdot}5$ and $L/W = 4$, $L = 100$ mm, $W = 25$ mm and $B = 12{\cdot}5$ mm. The predicted crack locations are compared with the actual values in Table 5. Figure 5 shows similar K versus β plots for cracks of different sizes with location at the centre of the beam. The comparison with actual values is presented in Table 6. The results for another set of data, $L/W = 6$, $L = 150$ mm, $W = 25$ mm, $B = 12{\cdot}5$ mm, are shown in Figure 6. The corresponding comparison of predicted and actual crack locations is given in Table 7.

3.3. CRACK EXTENSION MEASUREMENT

The natural frequencies at two crack lengths a_1 and a_2 are calculated using the finite element programme [17]. The results with and without the E correction described in section 2.3 are shown in Tables 8 and 9. Two different sets of geometric and material properties are used. These are included in the tables. The results clearly show the importance of the E correction. The errors without E correction are higher for smaller crack extensions.

4. EXPERIMENTAL STUDIES

4.1. SPECIMEN GEOMETRY AND EXPERIMENTAL SET-UP

Aluminium specimens from two different batches of material have been tested. Cross-sectional dimensions of the specimen are as follows:
Set 1: $W = 24{\cdot}5$ mm and $B = 12{\cdot}0$ mm.
Set 2: $W = 37{\cdot}5$ mm and $B = 12{\cdot}4$ mm.

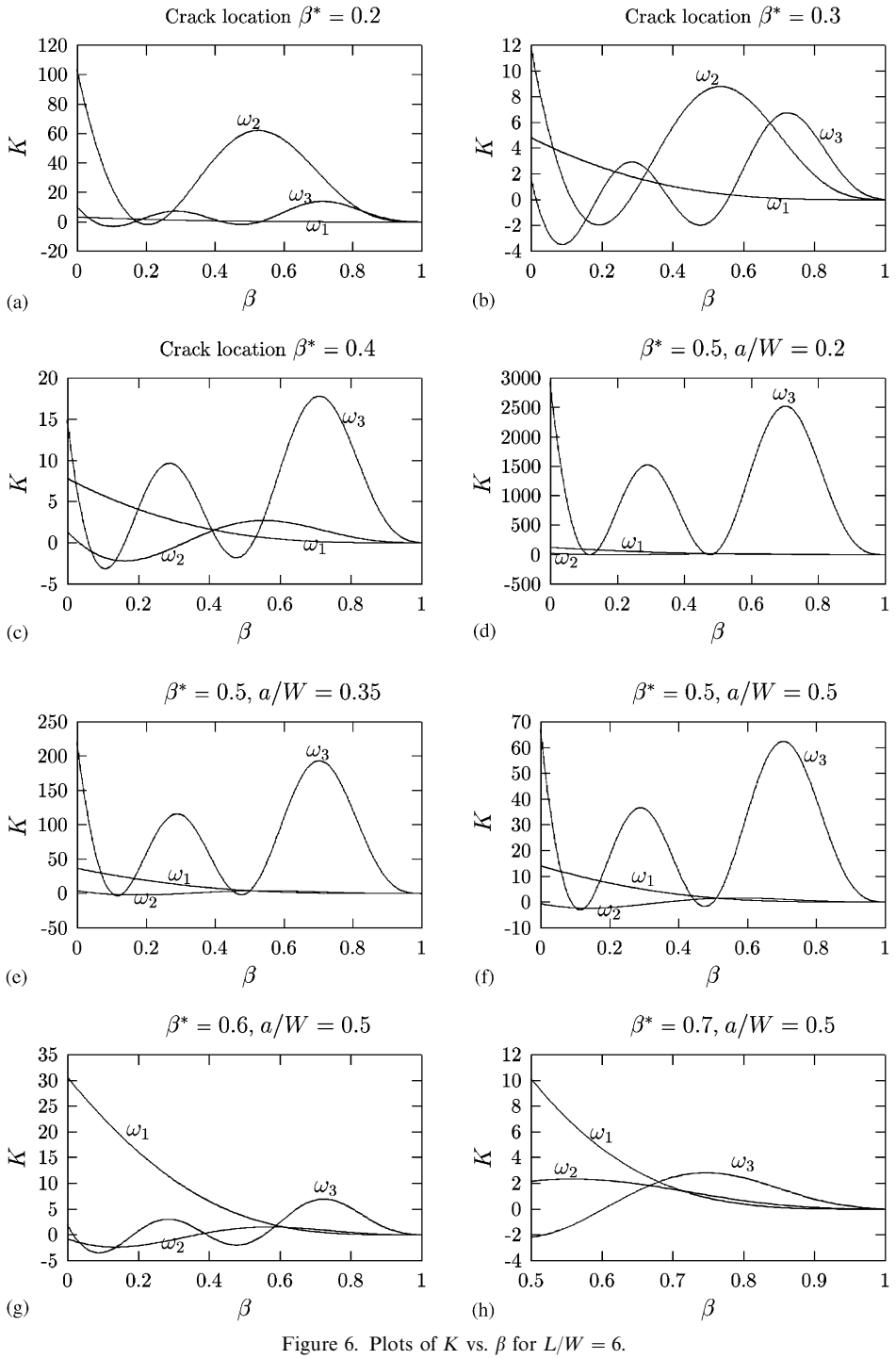

Figure 6. Plots of K vs. β for $L/W = 6$.

Several L/W ratios and crack locations (β^*) have been tested. This has been obtained by clamping each specimen at different positions. The modulus of elasticity E of the material has been determined experimentally through measurement of the first natural frequency. The details are given in the following section.

TABLE 5

Comparison of predicted and actual crack locations†

	Natural frequencies by FEM (Hz)			Predicted location	
β^*	ω_1	ω_2	ω_3	β	% Error
0·15	1200·98	9839·34	21433·8	0·144	− 0·6
0·20	1349·82	8600·40	21361·7	0·234	3·4
0·30	1513·96	7411·49	22268·4	0·349	4·9
0·40	1681·24	6701·47	22386·3	0·408	0·8
0·50	1829·36	6551·44	20065·8	0·523	2·3
0·60	1932·43	7069·81	17749·9	0·608	0·8
0·70	1982·38	8410·91	16529·9	0·702	0·2
0·80	1137·64	9534·87	22017·6	0·802	0·2

†$L = 100$ mm, $W = 25$ mm, $B = 12{\cdot}5$ mm, $a/W = 0{\cdot}5$.

TABLE 6

Comparison of predicted and actual crack locations ($\beta^* = 0{\cdot}5$)†

	Natural frequencies by FEM (Hz)			Predicted location	
β^*	ω_1	ω_2	ω_3	β	% Error
0·10	1987·02	9908·31	23263·1	0·513	1·3
0·20	1954·17	9364·59	23181·2	0·507	0·7
0·30	1810·41	7661·12	22767·4	0·510	1·0
0·40	1810·41	7661·12	22767·4	0·515	1·5

†$L = 100$ mm, $W = 25$ mm, $B = 12{\cdot}5$ mm

TABLE 7

Comparison of predicted and actual crack locations†

		Natural frequencies by FEM (Hz)			Predicted location	Error
a/W	β^*	ω_1	ω_2	ω_3	β	(%)
0·50	0·2	611·587	5033·12	11842·4	0·174	− 2·6
0·50	0·3	676·173	4671·33	11464·7	0·335	3·5
0·50	0·4	742·866	4048·12	11983·9	0·411	1·1
0·20	0·5	896·032	4810·61	12545·0	0·495	− 0·5
0·35	0·5	865·376	4321·77	12492·3	0·504	0·4
0·50	0·5	805·956	3681·89	12376·0	0·512	1·2
0·50	0·6	857·297	3638·62	11293·6	0·596	− 0·4
0·50	0·7	890·360	3946·15	10195·3	0·687	− 1·3

†$L/W = 6$, $L = 150$ mm, $W = 25$ mm, $B = 12{\cdot}5$ mm, $\beta^* = 0{\cdot}5$.

TABLE 8

Results for estimation of crack extension for set 1†

a_1/W	a_1 (mm)	a_2 (mm)	Natural freq. (Hz) ω_1	Natural freq. (Hz) ω_2	$(\Delta a)_{actual}$ (mm)	With E correction (Δa)	With E correction Error (%)	Without E correction (Δa)	Without E correction Error (%)
0·20	5·00	7·00	1954·16	1911·07	2·00	2·034	1·7	1·811	− 9·4
0·28	7·00	8·00	1911·07	1182·90	1·00	1·018	1·8	0·8716	− 12·8
0·36	9·00	10·00	1849·58	1810·41	1·00	1·028	2·8	0·9672	− 3·3
0·40	10·00	11·00	1810·41	1764·59	1·00	1·030	3·0	1·051	5·1
0·45	11·25	11·50	1751·98	1738·88	0·25	0·2615	4·6	0·2781	11·2
0·45	11·25	11·75	1751·98	1725·28	0·50	0·5217	4·3	0·5375	7·5
0·46	11·50	12·00	1738·88	1711·15	0·50	0·5225	4·5	0·5469	9·4
0·47	11·75	12·00	1725·28	1711·15	0·25	0·2627	5·0	0·2969	18·8
0·48	12·00	12·25	1711·15	1696·47	0·25	0·2634	5·3	0·3061	22·4
0·48	12·00	12·75	1711·15	1665·42	0·75	0·7847	4·6	0·8235	9·8
0·49	12·25	12·50	1696·47	1681·24	0·25	0·2638	5·5	0·3149	26·0
0·49	12·25	12·75	1696·47	1665·42	0·50	0·5248	5·0	0·5735	14·7
0·50	12·50	13·00	1681·24	1649·01	0·50	0·5252	5·0	0·5815	16·3
0·50	12·50	13·50	1681·24	1614·30	1·00	1·045	4·5	1·096	9·6
0·52	13·00	13·25	1649·00	1632·00	0·25	0·2643	5·7	0·3388	35·5
0·52	13·00	13·75	1649·00	1596·00	0·75	0·7848	4·6	0·8522	13·6
0·52	13·00	14·00	1649·00	1577·00	1·00	1·044	4·4	1·108	10·8
0·53	13·25	13·75	1632·00	1596·00	0·50	0·5252	5·0	0·6022	10·4
0·53	13·25	14·00	1632·0	1577·00	0·75	0·7845	4·6	0·8577	14·4
0·54	13·50	13·75	1614·2	1596·00	0·25	0·2631	5·2	0·3522	40·9
0·54	13·50	14·0	1614·3	1577·0	0·50	0·5230	5·6	0·6077	21·5
0·55	13·75	14·0	1596·0	1577·0	0·25	0·2645	5·8	0·3577	43·1
0·55	13·75	15·0	1596·0	1493·75	1·25	1·295	3·6	1·370	9·6
0·56	14·00	15·0	1577·0	1493·74	1·00	1·036	3·6	1·120	12·0
0·60	15·00	17·0	1493·75	1289·21	2·00	2·012	0·6	2·087	4·35

†$L = 100$ mm, $W = 25$ mm, $B = 12{\cdot}5$ mm, $E = 210$ GPa, $\rho = 7860$ kg/m^3, $\nu = 0{\cdot}3$.

4.1.1. *Measurement of modulus of elasticity*

For an uncracked cantilever beam, the natural frequencies based on the Timoshenko beam theory are given by [16]

$$2 + [b^2(r^2 - s^2)^2 + 2]\cosh bp \cos bq - \frac{b(r^2 + s^2)}{(1 - b^2r^2s^2)^{1/2}} \sinh bp \sin bq = 0. \tag{39}$$

The above equation is solved for the frequency parameters b corresponding to the first natural frequencies for a set of beams. The modulus of elasticity is calculated through equation (7) using b and measured natural frequency ω. A number of readings have been taken considering different length to width ratios. Finally, the average is employed for further calculations. The moduli for the two sets of material are obtained as 58·5 and 58·9 GPa respectively.

4.1.2. *Manufacture of cracked specimen*

The specimen was cut to size from ready-made rectangular bars. The crack was introduced by wire cut machining. The wire diameter is 0·25 mm. The width of the slot

TABLE 9

Results for estimation of crack extension for set 2†

a_1/W	a_1 (mm)	a_2 (mm)	*Natural freq. (Hz)* ω_1	ω_2	$(\Delta a)_{actual}$ (mm)	*With E* correction (Δa)	Error (%)	Without *E* correction (Δa)	Error (%)
0·449	11·0	11·1	719·53	718·10	0·10	0·0997	− 0·33	0·01267	− 87·33
0·449	11·0	11·6	719·53	710·54	0·60	0·6088	1·47	0·53020	− 11·63
0·449	11·0	12·4	719·53	696·93	1·40	1·4220	1·57	1·35500	− 3·21
0·453	11·1	11·6	718·10	710·54	0·50	0·5073	1·46	0·43020	− 13·96
0·453	11·1	13·1	718·10	683·26	2·00	2·0310	1·55	1·97500	− 1·25
0·473	11·6	11·8	710·54	683·26	0·20	0·2024	1·20	0·13700	− 31·50
0·473	11·6	12·9	710·54	687·34	1·30	1·3210	1·62	1·27000	− 2·31
0·482	11·8	12·3	707·32	698·74	0·50	0·5082	1·64	0·45260	− 9·48
0·502	12·3	12·4	698·74	696·93	0·10	0·1009	0·90	0·05549	− 44·51
0·502	12·3	12·9	698·74	687·34	0·60	0·6107	1·78	0·57000	− 5·00
0·506	12·4	12·9	696·93	687·34	0·50	0·5091	1·82	0·47000	− 6·00
0·506	12·4	13·4	696·93	676·85	1·00	1·0150	1·50	0·98100	− 1·90
0·527	12·9	13·1	687·34	683·26	0·20	0·2028	1·40	0·17470	− 12·65
0·527	12·9	13·4	687·34	676·85	0·50	0·5073	1·46	0·48100	− 3·80
0·535	13·1	13·4	683·26	676·85	0·30	0·3042	1·40	0·28100	− 6·33
0·535	13·1	13·5	683·26	674·63	0·40	0·4056	1·40	0·38300	− 4·25
0·547	13·4	13·5	676·85	674·63	0·10	0·1012	1·20	0·08303	− 16·97

†$L = 160$ mm, $W = 24{\cdot}5$ mm, $B = 12$ mm, $E = 70$ GPa, $\rho = 2645$ kg/m^3, $v = 0{\cdot}33$.

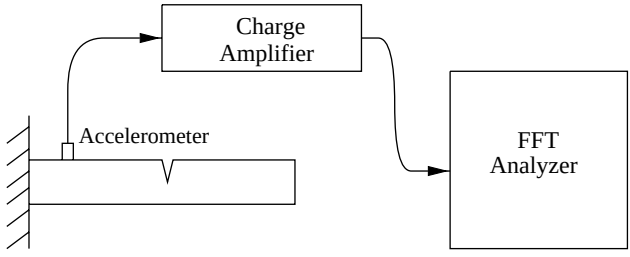

Figure 7. Schematic diagram of experimental set-up.

obtained thereby is 0·28 mm. In some cases, cracks are made with a thin hacksaw. The slot obtained thereby is approximately of width 1 mm.

4.1.3. *Experimental procedure*

Figure 7 shows the schematic diagram of the experimental set-up. The specimen is clamped at one end. The beam is excited by hitting it lightly with an instrumentation hammer. A very light weight accelerometer (0·65 g, B&K make, accelerometer type 4374) is fixed on the beam near the clamped end to monitor its vibration. The natural frequencies are obtained by using an FFT analyser (Advantest R9211A).

4.2. FORWARD PROBLEM

The material density and the Poisson ratio were taken [19, 20] as $\rho = 2645$ kg/m^3 and $v = 0{\cdot}33$ respectively. The beam dimensions are included in the tables mentioned later. The natural frequencies of the beams were calculated from the characteristic equation (33).

TABLE 10

Comparison of analytical and experimental natural frequencies

		Natural frequencies (Hz)								
		Analytical			Experimental			% Error		
L/W	β^*	ω_1	ω_2	ω_3	ω_1	ω_2	ω_3	in ω_1	in ω_2	in ω_3
$W = 24{\cdot}5$ mm, $B = 12$ mm, $a/W = 0{\cdot}506$, $E = 58{\cdot}5$ GPa, $\rho = 2645$ kg/m^3, $\nu = 0{\cdot}33$										
3·673	0·100	1142·1	10212	23981	1205·0	10300	23300	5·22	0·85	2·92
4·082	0·200	1071·2	9023·6	19055	1100·0	7850·0	17800	2·62	14·95	7·05
4·694	0·304	956·68	6613·3	14850	956·0	5650·0	14950	0·07	17·05	0·67
5·429	0·398	819·13	4543·2	12861	820·0	4175·0	13050	0·11	8·82	1·45
5·918	0·448	733·32	3711·3	11708	722·5	3612·5	11450	1·50	2·73	2·25
6·531	0·500	636·41	3023·5	10020	637·5	3000·0	9900	0·17	0·78	1·21
$W = 37{\cdot}5$ mm, $B = 12{\cdot}4$ mm, $a/W = 0{\cdot}4053$, $E = 58{\cdot}9$ GPa, $\rho = 2645$ kg/m^3, $\nu = 0{\cdot}33$										
5·067	0·153	553·27	4081·2	9717·6	542·5	4100	9650	1·99	0·46	0·70
5·360	0·199	521·16	3760·7	8542·1	512·5	3675	8750	1·69	2·33	2·38
6·133	0·300	441·49	2841·2	6594·1	436·25	2850	6625	1·20	0·31	0·47
7·147	0·399	376·90	1906·5	5997·5	352·5	1925	5700	6·92	0·96	5·22
6·267	0·149	381·14	2807·2	6999·0	376·25	2837·5	7000	1·30	1·07	0·01
6·667	0·200	354·57	2560·0	6051·9	355·0	2463	6250	0·12	3·94	3·17
7·120	0·251	325·98	2252·5	5210·4	311·25	2137·5	5175	4·73	5·38	0·68
7·627	0·301	296·31	1928·3	4602·4	283·75	1750	4725	4·43	10·19	2·59

Three different beams are tested. Two of the beams have the same cross-sectional area and material properties. During testing, the clamping position is changed to obtain a variation in L/W and crack location β^*. The Newton–Raphson iteration technique has been used for the solution. These analytical and experimental results are compared in Table 10. The experimental results are in good agreement with the analytical results. The error in the second mode natural frequency is the highest. This trend confirms the results of the numerical studies.

4.3. INVERSE PROBLEM

The dimensional combinations considered for the verification of the inverse problem are the same as those in the earlier section. The crack location was predicted using the experimentally measured natural frequencies. The plots of K against β are presented in Figures 8 and 9. A comparison of predicted and actual crack location is presented in Tables 11 and 12 respectively.

The predicted results are in good agreement with the actual values. The error is $< 10\%$. But in some cases, e.g., Figures 8(b) and 9(e), the three K versus β curves do not intersect in a single point. In the first case (Figure 8(b)), the midpoint of the shortest distance between the two non-intersecting curves (ω_1 and ω_3) is considered to be the intersection point for the pair. In the case of Figure 9e, the midpoint of the two intersections [(ω_1 and ω_2) and (ω_1 and ω_3)] is taken to correspond to the crack location.

4.4. ESTIMATION OF CRACK EXTENSION

The method has been tested for two beams with different geometry and material data. The crack is located at the centre of the beams in both the cases. The cracks have been cut

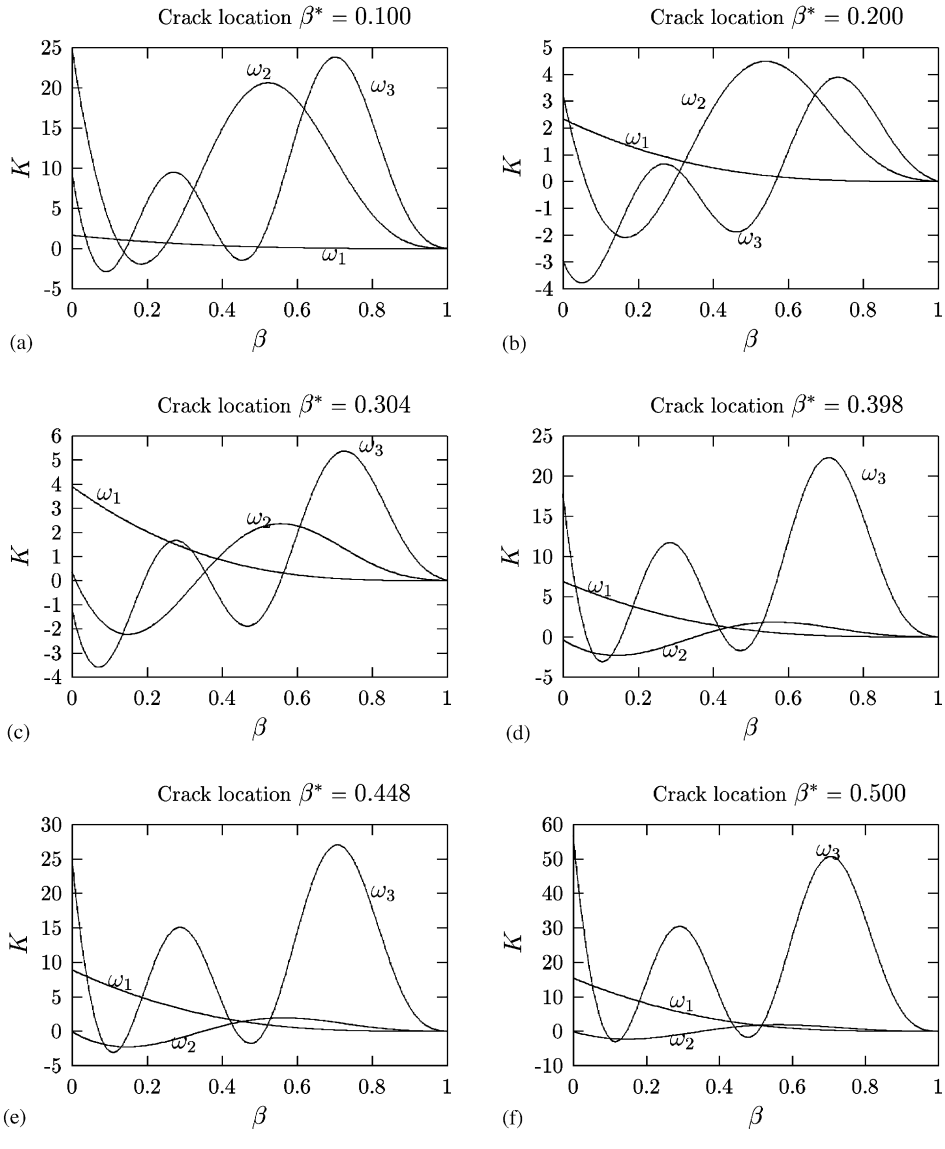

Figure 8. Plots of K vs. β for Case 1.

with a thin hacksaw. Whenever the crack is extended, it is done using again the same hacksaw and without removing the specimen from the experimental set-up. E correction is employed as usual. The results are presented in Tables 13 and 14. The maximum error in the estimation of crack extension is 33·8%. A part of this high error can be attributed to the fact that the hacksaw cut does not correspond to a sharp crack as can be obtained through fatigue pre-cracking.

5. CONCLUSIONS

Vibration-based methods have been extended to short beams taking into account the effects of rotational inertia and shear deformation. A method to measure a change in crack

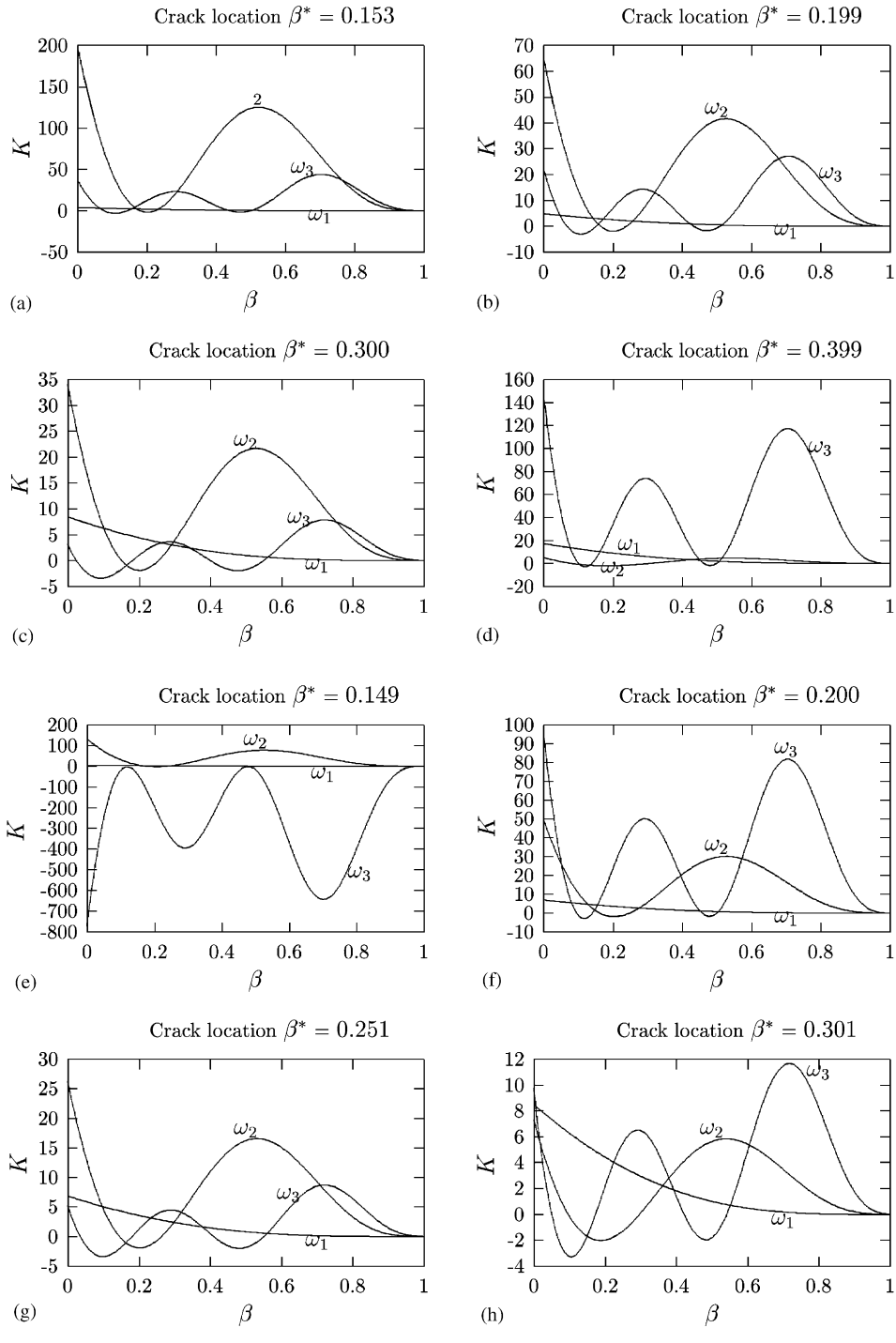

Figure 9. Plots of K vs. β for Case 2.

length from the change in the first natural frequency has been presented. The details of the methods have been given. The accuracy of the methods is illustrated by case studies involving a short cantilever beam with a crack. Both numerical and experimental case

TABLE 11

Comparison of predicted and actual crack locations for Case 1†

Corresponding K versus β plot	L/W	Actual crack location (β*)	Experimental natural freq. (Hz)			Predicted location (β)	Error (%)
			ω_1	ω_2	ω_3		
Figure 8(a)	3·673	0·100	1205·0	10300	23300	0·138	3·8
Figure 8(b)	4·082	0·200	1100·0	7850·0	17800	0·283	8·3
Figure 8(c)	4·694	0·304	956·0	5650·0	14950	0·353	4·9
Figure 8(d)	5·429	0·398	820·0	4175·0	13050	0·424	2·6
Figure 8(e)	5·918	0·448	722·5	3612·5	11450	0·433	− 1·5
Figure 8(f)	6·531	0·500	637·5	3000·0	9900	0·513	1·3

†$W = 24{\cdot}5$ mm, $B = 12$ mm, $a/W = 0{\cdot}506$, $E = 58{\cdot}5$ GPa.

TABLE 12

Comparison of predicted and actual crack locations for Case 2†

Corresponding K versus β plot	L/W	Actual crack location (β*)	Experimental natural freq. (Hz)			Predicted location (β)	Error (%)
			ω_1	ω_2	ω_3		
Figure 9(a)	5·067	0·153	542·5	4100	9650	0·164	1·1
Figure 9(b)	5·360	0·199	512·5	3675	8750	0·158	− 4·1
Figure 9(c)	6·133	0·300	436·25	2850	6625	0·284	− 1·6
Figure 9(d)	7·147	0·399	352·5	1925	5700	0·441	4·1
Figure 9(e)	6·267	0·149	376·25	2837·5	7000	0·123	− 2·6
Figure 9(f)	6·667	0·200	355·0	2463	6250	0·144	− 5·6
Figure 9(g)	7·120	0·251	311·25	2137·5	5175	0·332	8·1
Figure 9(h)	7·627	0·301	283·75	1750	4725	0·378	7·7

†$W = 37{\cdot}5$ mm, $B = 12{\cdot}4$ mm, $a/W = 0{\cdot}405$, $E = 58{\cdot}9$ GPa.

TABLE 13

Experimental results for estimation of crack extension for Case 1†

a_1 (mm)	a_2 (mm)	$(\Delta a)_{actual}$ (mm)	Natural freq. (Hz)		$(\Delta a)_{estimated}$ (mm)	Error (%)
			ω_1	ω_2		
10·6	11·4	0·8	685·0	667·5	1·21	33·1
10·6	12·2	1·6	685·0	660·0	1·71	6·9
10·6	13·7	3·1	685·0	637·5	2·91	− 6·8
10·6	14·8	4·2	685·0	627·5	3·37	− 19·1
10·6	15·5	4·9	685·0	607·5	4·18	− 14·7
12·2	13·7	1·5	660·0	637·5	1·21	− 19·3
12·2	14·8	2·6	660·0	627·5	1·72	− 33·8
12·2	15·5	3·3	660·0	607·5	2·61	− 20·9
13·7	15·5	1·8	637·5	607·5	1·20	− 33·0
14·8	15·5	0·7	627·5	607·5	0·64	− 9·1

†$L = 160$ mm, $W = 24{\cdot}5$ mm, $B = 12$ mm, $E = 58{\cdot}5$ GPa.

TABLE 14

Experimental results for estimation of crack extension for Case 2[†]

a_1 (mm)	a_2 (mm)	$(\Delta a)_{actual}$ (mm)	Natural freq. (Hz)		$(\Delta a)_{estimated}$ (mm)	Error (%)
			ω_1	ω_2		
11·4	13·8	2·4	735·0	725·0	2·140	− 10·8
11·4	16·7	5·3	735·0	707·5	4·097	− 22·7
11·4	19·2	7·8	735·0	690·0	5·716	− 26·7
11·4	20·7	9·3	735·0	667·5	7·458	− 19·8
13·8	16·7	2·9	725·0	707·5	2·343	− 19·2
13·8	19·2	5·4	725·0	690·0	3·851	− 28·3
13·8	20·7	6·9	725·0	667·5	5·491	− 18·8
16·7	19·2	2·5	707·5	690·0	1·700	− 32·0
16·7	20·7	4·0	707·5	667·5	3·203	− 19·9

[†]$L = 180$ mm, $W = 37{\cdot}5$ mm, $B = 12{\cdot}4$ mm, $E = 58{\cdot}9$ GPa.

studies are presented. From the range of crack locations and sizes considered in the numerical studies, the errors in prediction of natural frequencies are observed to be $< 1\%$ for the first mode of vibration for beams with $L/W \geqslant 3$. For the second and third mode, the errors are of the order of 10%. The errors in detection of crack location and estimation of crack extension are $< 10\%$. Based on the experimental study, the errors in the prediction of natural frequencies and detection of crack location are of the order of 10%. The maximum error in estimation of crack extension is about 34%. The results are encouraging. This may enthuse using the method for measurement of crack extension during fatigue crack growth studies using the three-point bend specimen.

REFERENCES

1. H. J. PETROSKI 1981 *International Journal of Fracture* **17**, R71–R76. Simple static and dynamic models for the cracked elastic beam.
2. C. A. PAPADOPOULOS and A. D. DIMAROGONAS 1987 *Journal of Sound and Vibration* **117**, 81–93. Coupled longitudinal and bending vibrations of a rotating shaft with an open crack.
3. T. G. CHONDROS and A. D. DIMAROGONAS 1980 *Journal of Sound and Vibration* **69**, 531–538. Identification of cracks in welded joints of complex structures.
4. P. F. RIZOS, N. ASPRAGATHOS and A. D. DIMAROGONAS 1990 *Journal of Sound and Vibration* **138**, 381–388. Identification of crack location and magnitude in a cantilever beam from the vibration modes.
5. S. CHRISTIDES and A. D. S. BARR 1984 *International Journal of Mechanical Science* **26**, 639–648. One-dimensional theory of cracked Bernoulli–Euler beams.
6. T. G. CHONDROS and A. D. DIMAROGONAS 1998 *Journal of Sound and Vibration* **215**, 17–34. A continuous cracked beam vibration theory.
7. T. R. CHANDRUPATLA and A. D. BELEGUNDU 1997 New Delhi; Prentice Hall of India. *Introduction to Finite Elements in Engineering*.
8. G. GOUNARIS and A. D. DIMAROGONAS 1988 *Computers and Structures* **28**, 309–313. A finite element of cracked prismatic beam for structural analysis.
9. R. Y. LIANG, F. K. CHOY, and J. HU 1991 *Journal of the Franklin Institute* **328**, 505–518. Detection of cracks in beam structures using measurements of natural frequencies.
10. B. P. NANDWANA and S. K. MAITI 1997 *Journal of Sound and Vibration* **203**, 435–446. Detection of location and size of a crack in stepped cantilever beam based on measurement of natural frequencies.

11. B. P. NANDWANA and S. K. MAITI 1997 *Engineering Fracture Mechanics* **58**, 193–205. Modelling of vibration of beam in presence of inclined edge or internal crack for its possible detection based on frequency measurement.
12. T. D. CHAUDHARI and S. K. MAITI 2000 *International Journal of Solids and Structures* **37**, 761–779. A study of vibration of geometrically segmented beams with and without cracks.
13. T. C. TSAI and Y. Z. WANG 1996 *Journal of Sound and Vibration* **192**, 607–620. Vibration analysis and dignostics of a cracked shaft.
14. W. M. OSTACHOWICZ and M. KRAWCZUK 1991 *Journal of Sound and Vibration* **150**, 191–201. Analysis of the effect of cracks on the natural frequencies of a cantilever beam.
15. S. TIMOSHENKO, D. H. YOUNG, and W. WEAVER JR 1967 *Vibration Problems in Engineering*. New York: John Wiley & Sons.
16. T. C. HUANG 1961 *Journal of Applied Mechanics, Transactions of American Society of Mechanical Engineers* **53,** 579–584. The effect of rotary inertia and of shear deformation on the frequency and normal mode equations of uniform beams with simple end conditions.
17. S. K. MAITI 1996 *Technical Report, Department of Mechanical Engineering, Indian Institute of Technology, Bombay*. Finite element package for stress and vibration analysis.
18. K. J. BATHE 1990 *Finite Element Procedures in Engineering Analysis*. New Delhi; Prentice-Hall. India.
19. T. D. CHAUDHARI 2000 *Ph.D. Thesis, Department of Mechanical Engineering, Indian Institute of Technology, Bombay*. Modelling of transverse vibration of geometrically segmented beams to facilitate crack detection.
20. B. P. NANDWANA 1997 *Ph.D Thesis, Department of Mechanical Engineering, Indian Institute of Technology, Bombay*. On foundation for detection of crack based on measurement natural frequencies.